Quantum mechanical study of the $F + D_2 \rightarrow DF + D$ reaction

Pascal Honvault, Jean-Michel Launay

PALMS, UMR 6627 du CNRS, Université de Rennes 1, Campus de Beaulieu, 35042 Rennes Cedex, France

Abstract

A quantum-mechanical calculation of differential and integral cross sections for the $F + D_2(v=0, j=0,1,2) \rightarrow DF(v'j') + D$ reaction has been performed using the ab initio potential energy surface of Stark and Werner. The hyperspherical method has been used and results have been obtained at two collision energies (90 and 140 meV). Bimodal rotational distributions for backward scattering and a forward scattering for $v'=4$ have been found, in semi-quantitative agreement with recent crossed beam experiments. © 1998 Elsevier Science B.V. All rights reserved.

1. Introduction

The $F + H_2 \rightarrow HF + H$ reaction has been studied theoretically several times in the last 20 years. It is now considered as a benchmark for potential energy surfaces and dynamical calculations on atom–diatom reactive systems. Theoretical studies have been stimulated by the crossed molecular beam experiments of Lee and co-workers who have obtained vibrationally resolved differential cross sections (DCS) for the $F + H_2$ [1], $F + D_2$ and $F + HD$ [2] systems. For $F + H_2$, quasi-classical trajectory (QCT) [3,4] and quantum mechanical [5–8] calculations with different potential energy surfaces (T5A, TS, 5-SEC, 6-SEC) [9–12] have reproduced qualitatively the experimental results. The best agreement, especially for DCS and rate coefficients, is obtained with the recent ab initio potential energy surface of Stark, Werner and co-workers (SW) [13–19].

The $F + D_2$ system has been studied less often theoretically than its isotopic variant. However, re-

newed interest has happened because of high resolution crossed molecular beam experiments performed in Göttingen. These have yielded absolute differential and integral cross sections for collision energies ranging from 83 to 240 meV [20–24] and more recently, rotational distributions [25]. Theoretical results have been obtained on the SW potential energy surface, using the QCT method for the initial ($v=0, j=0,1,2$) D_2 states [26,27] and a coupled states (CS) quantum-mechanical approximation [24,25] for the initial ($v=0, j=0$) D_2 state,

There are quantitative and even qualitative differences between experimental and theoretical results. Firstly, experiments at 140 meV [21,23] show a forward peak for $DF(v'=4)$ [26,28] and a backward maximum whose magnitudes are underestimated in QCT calculations. At somewhat lower energies (79 or 90 meV), no forward peak is observed experimentally [2] nor in QCT calculations [26,28] whereas the CS method yields a forward maximum for $v'=3$ [24,25]. Secondly, at 90 meV, bimodal rotational distributions for backward scattering have been ob-

served for $v' = 2$ and 3, whereas CS shows bimodal distributions for $v' = 1$, 2 and 3 [25] and QCT does not show any bimodal distributions [28].

For these reasons, we have undertaken a quantum mechanical study of the $F + D_2$ $(v = 0, j = 0,1,2)$ reaction with the SW surface at 90 and 140 meV to ascertain the dependence on initial rotational state, the importance of the forward peak and the existence of bimodal rotational distributions.

2. Scattering calculations

Details of the hyperspherical method can be found in Refs. [5,6,29,30] and only a brief description is given here. Nuclear motion in the FDD system are represented by a set of coordinates which are a modified version of the Smith–Whitten democratic coordinates. They consist of three Euler angles, representing the orientation of the triatomic system in space and three internal coordinates: the hyperradius ρ, which characterises the size of the system and two hyperangles which characterise its shape.

We first compute a set of surface states $\Phi_k(\rho; \theta, \phi)$, eigenfunctions of a fixed-ρ reference hamiltonian which incorporates the potential energy and kinetic energies arising from deformation and rotation around the axis of least inertia. They are also eigenfunctions of the angular momentum projection Ω onto the axis of least inertia, of inversion and of the DD permutation operator. The Φ_k states are expanded onto a basis of pseudo hyperspherical harmonics built from trigonometric functions [31]. At large ρ, they concentrate into the arrangement valleys at small θ and a contraction scheme [6] can be used to reduce the size of the expansion basis by a factor of roughly 2. The size of the expansion basis varies between 500 and 3000 depending on ρ and Ω. The range of variation of the hyperradius is divided into 46 equal sectors between 2.1 and 11.3 a_0 where the Φ_k basis dissociates into the DF (40,37,33,29,25,19,11) and D_2 (14,10,3) rovibrational sets (this notation indicates the largest rotational level j for each vibrational manifold $v = 0,1,....$ Two vibrational manifolds in each arrangement ($v = 5,6$ for DF and $v = 1,2$ for D_2) correspond to closed channels.

We then perform a close-coupling expansion of the full FDD wavefunction onto the surface states.

The hyperradial components satisfy a set of second-order coupled differential equations in which all couplings neglected in the first step are taken into account. The logarithmic derivative matrix is propagated inside each sector using the Johnson-Manolopoulos algorithm [32]. Basis transformations are performed at the boundary between sectors and at large hyperradius, the numerically integrated wavefunction is matched onto a set of regular and irregular asymptotic functions expressed in the laboratory frame. The K and S-matrices are extracted and integral and differential cross sections are obtained from standard equations.

Production runs were performed with all surface surface states with $|\Omega| \leq 7$ and all partial waves with $J \leq 30$ in the close-coupling expansion (1480 channels for symmetric functions and 1490 channels for antisymmetric functions). A test calculation with all states with $|\Omega| \leq 10$ produced graphically identical differential cross sections. The computation of surface states is roughly 10 times more expensive than for the similar FHH system with the T5A surface [5,6], and the solution of the close coupling equations 5 times more expensive.

3. Results and discussion

We first generated state to state DCS $d\sigma/d\Omega|_{v=0j \rightarrow v'j'}(\Theta)$ for two scattering energies (90 meV and 140 meV). Θ is the center of mass scattering angle, $\Theta = 0°$ corresponding to forward scattering and $\Theta = 180°$ to backward scattering. The theoretical DCS have then been averaged over the initial rotational state distribution of the crossed beam experiment, i.e. 90% $j = 0$ and 10% $j = 1$ for 90 meV, 85% $j = 0$, 10% $j = 1$ and 5% $j = 2$ for 140 meV [23,25]. These averaged DCS are denoted as $d\sigma/d\Omega|_{v=0 \rightarrow v'j'}(\Theta)$. We also summed these DCS over the final rotational state j' to obtain the rotationally summed DCS $d\sigma/d\Omega|_{v=0 \rightarrow v'}(\Theta)$. All calculated cross sections have been multiplied by a factor of 0.5 to account for the population of the $^2P_{3/2,3/2}$ fine-structure state of F which does not react and is not considered in this calculation.

Fig. 1 shows the rotationally summed DCS and the experimental results [23,28] at 90 meV (Fig. 1.a) and 140 meV (Fig. 1.b). Experimental uncertainties are within 10% for the relative magnitudes and
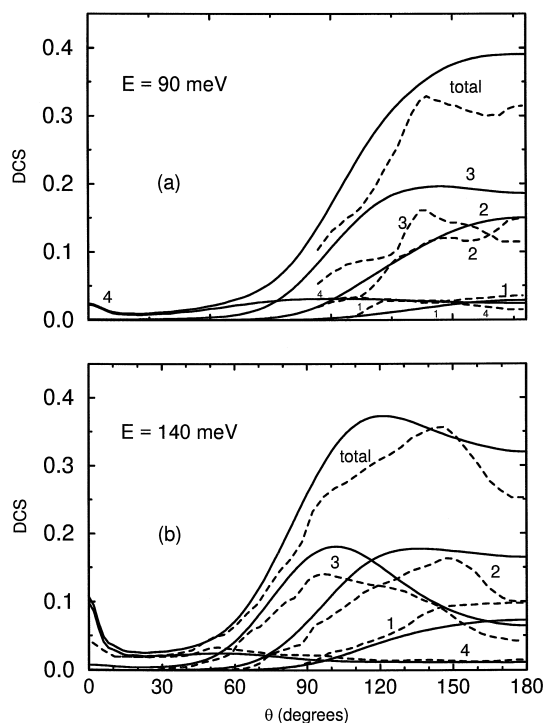
Fig. 1. Rotationally summed DCS $d\sigma/d\Omega|_{v=0 \rightarrow v'}(\Theta)$ (in Å^2/sr) as a function of the center of mass scattering angle Θ. Full lines: present results. Dashed lines : experimental results [23,28]. For $E = 90$ meV, experimental results are available only for $\Theta > 90°$.

within 50% for the absolute magnitudes [23]. At 90 meV, the theoretical DCS are backward peaked for $v' = 1,2$ and 3 and show a sideways broad maximum for $v' = 4$. A forward peak in the total DCS is also present, it is due to scattering in $v' = 4$. It cannot be compared to the experiment because Toennies and co-workers did not measure the $v' = 4$ DCS for $\Theta < 90°$ at this energy. At 140 meV, the DCS move to smaller scattering angles. A sideways maximum at 105° appears for $v' = 3$. The intensity of the $v' = 4$ forward peak increases with energy and it is clearly seen, though with less intensity, in the experiment. There is thus a semi-quantitative agreement with experiment, both in the relative magnitude of the DCS, their angular dependence and their variation with scattering energy. However, the experimental DCS show some broad undulations as a function of the scattering angle whereas the theoretical DCS are very smooth functions of Θ.

We compare our results with other theoretical works. Approximate CS results by Baer et al. [24,25]

obtained for $j = 0$ at 87 meV show a forward peak mainly due to scattering for $v' = 3$ and not $v' = 4$. QCT results by Aoiz et al. [26,28], in contrast with ours, depend strongly on the initial rotational state j. They show almost no forward scattering at 90 meV for the initial rotational state $j = 0$, and some $v' = 4$ forward scattering at 140 meV in the least populated rotational states $j = 1,2$. This confirms the idea that the forward peak for $v' = 4$, as in F + H$_2$ (for $v' = 3$), is due to tunnelling effects through the centrifugal barrier of the entrance valley [18]. Moreover, QCT calculations underestimate the magnitude of the DCS for backward scattering. Finally, as in our work, no undulations are present in the QCT and CS differential cross sections.

Table 1 shows the integral cross sections $\sigma_{v=0 \rightarrow v'}$ at the two scattering energies. The largest discrepancies with experiment occur for $v' = 1$ and $v' = 3$ at 90 meV, whereas there is a better overall agreement at 140 meV. Our results at 90 meV agree better with the approximate CS results than with the QCT ones, which underestimate the $v' = 1$ cross section and overestimate the $v' = 4$ cross sections.

Fig. 2 shows the 90 meV state to state DCS $d\sigma/d\Omega|_{v=0 \rightarrow v'j'}(\Theta)$ plotted as a function of Θ and j' for several values of the final vibrational quantum number v'. Theoretical DCS for $v' = 1,2$ and 3 show rotational bimodal distributions for backward scattering. This bimodal distribution disappears gradually at

Table 1
Integral cross sections $\sigma_{v=0 \rightarrow v'}$ (in Å^2)

	This work	Experiment [a]	CS [b]	QCT [c]
$v' = 1$	(0.06) 0.06	(0.11) 0.11	(0.08) 0.08	0.02
	0.26	0.35	–	0.34
$v' = 2$	(0.42) 0.45	(0.43) 0.43	(0.59) 0.63	0.40
	1.03	0.80	–	1.00
$v' = 3$	(0.90) 1.03	(0.61) 0.68	(0.65) 0.77	0.85
	1.24	1.01	–	0.92
$v' = 4$	(0.17) 0.29	(0.20) 0.28	(0.22) 0.31	0.42
	0.22	0.26	–	0.28
Total	(1.55) 1.83	(1.35) 1.50	(1.54) 1.79	1.69
	2.75	2.40	–	2.54

Refs. [23,25]. [b] Refs. [23,25]. [c] Ref. [23]. For each value of v', the upper entries are for 90 meV and the lower entries are for 140 meV. At 90 meV, the results in parentheses denote the contribution of scattering angles between 90° and 180° to the integral cross section. Results without parentheses show the contribution of all scattering angles. Experimental results for $\Theta < 90°$ are taken from Ref. [2].
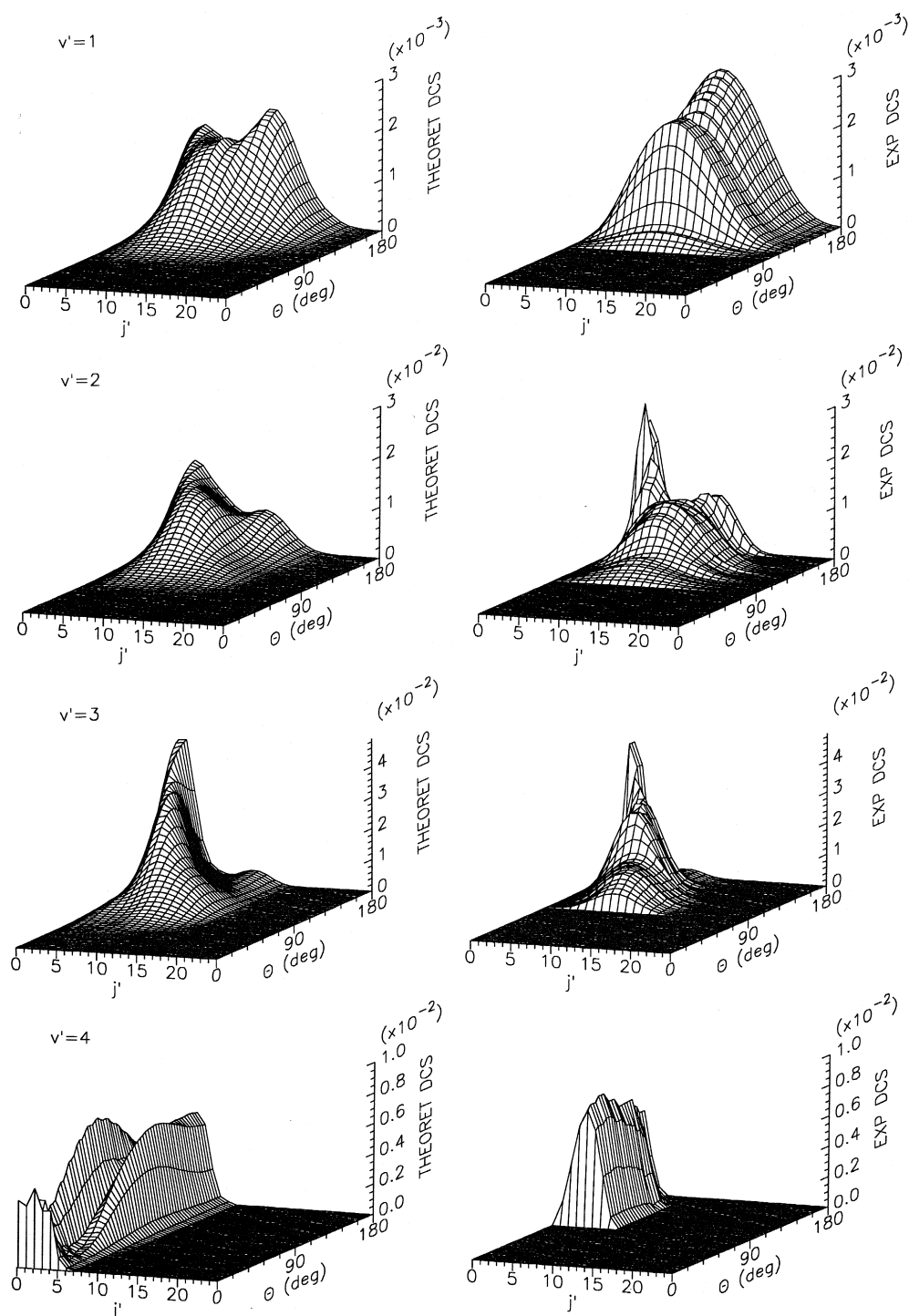
Fig. 2. Three-dimensional plots of the state-to-state differential cross section $d\sigma/d\Omega|_{v=0 \rightarrow v'j'}(\Theta)$ (in $\text{Å}^2/\text{sr}$) at 90 meV as a function of the scattering angle Θ and the final rotational quantum number j'. The column on the left shows the present results and the column on the right the experimental ones generated using the analytical representation of Refs. [23,28]. Experimental results are available only for $\Theta > 90°$.

smaller scattering angles. For $v' = 3$, the maximum of the rotational distribution shifts to higher j'. This behaviour has already been found in the Cl + H_2 → HCl ($v' = 0,1$) + H reaction [33], but for larger scattering energies (0.5 and 0.75 eV). The $v' = 4$ DCS is more complicated, with a bimodal rotational distribution for sideways scattering and a monomodal distribution for backward scattering ($140° < \Theta < 180°$). It also shows fast but small amplitude oscillations as a function of Θ for small j'. Experimental DCS also show bimodal rotational distributions in the $v' = 2$ and $v' = 3$ final vibrational states for backward scattering, whereas the $v' = 1$ and $v' = 4$ distributions have a monomodal character (for $\Theta > 90°$).

Acknowledgements

References

[1] D.M. Neumark, A.M. Wodtke, G.N. Robinson, C. Hayden, Y.T. Lee, J. Chem. Phys. 82 (1985) 3045.
[2] D.M. Neumark, A.M. Wodtke, G.N. Robinson, C. Hayden, R. Shobatake, R.K. Sparks, T.P. Shafer, Y.T. Lee, J. Chem. Phys. 82 (1985) 3067.
[3] F.J. Aoiz, L. Banares, V.J. Herrero, V. Saez Rabanos, Chem. Phys. Lett. 218 (1994) 422.
[4] F.J. Aoiz, L. Banares, V.J. Herrero, V. Saez Rabanos, Chem. Phys. 187 (1994) 227.
[5] J.M. Launay, Theor. Chim. Acta 79 (1991) 183.
[6] J.M. Launay, M. Le Dourneuf, Chem. Phys. Lett. 169 (1990) 473.
[7] E. Rosenman, S. Hochman-Kowal, A. Persky, M. Baer, J. Phys. Chem. 99 (1995) 16523.
[8] S.E. Bradford, D.W. Arnold, D.M. Neumark, D.E. Manolopoulos, J. Chem. Phys. 99 (1993) 6345.
[9] R. Steckler, D.G. Truhlar, B.C. Garrett, J. Chem. Phys. 82 (1985) 5499.
[10] T. Takayanagi, S. Sato, Chem. Phys. Lett. 144 (1988) 191.
[11] G.C. Lynch, R. Steckler, D.W. Schwenke, A.J.C. Varandas, D.G. Truhlar, B.C. Garrett, J. Chem. Phys. 94 (1991) 7136.
[12] S.L. Mielke, G.C. Lynch, D.G. Truhlar, D.W. Schwenke, Chem. Phys. Lett. 213 (1993) 10; 217 (1994) 173.
[13] K. Stark, H.-J. Werner, J. Chem. Phys. 104 (1996) 6515.
[14] F.J. Aoiz, L. Banares, V.J. Herrero, V. Saez Rabanos, K. Stark, H.-J. Werner, Chem. Phys. Lett. 223 (1994) 215.
[15] F.J. Aoiz, L. Banares, V.J. Herrero, V. Saez Rabanos, K. Stark, H.-J. Werner, J. Chem. Phys. 102 (1995) 9248.
[16] F.J. Aoiz, L. Banares, V.J. Herrero, K. Stark, H.-J. Werner, Chem. Phys. Lett. 254 (1996) 341.
[17] E. Rosenman, S. Hochman-kowal, A. Persky, M. Baer, Chem. Phys. Lett. 257 (1996) 421.
[18] J.F. Castillo, D.E. Manolopoulos, K. Stark, H.-J. Werner, J. Chem. Phys. 104 (1996) 6531.
[19] P. Honvault, J.M. Launay, to be published.
[20] M. Faubel, L. Rusin, S. Schlemmer, F. Sondermann, U. Tappe, J.P. Toennies, J. Chem. Phys. 101 (1994) 2106.
[21] M. Faubel, B. Martínez-Haya, L.Y. Rusin, U. Tappe, J.P. Toennies, Chem. Phys. Lett. 232 (1995) 197.
[22] M. Faubel, B. Martínez-Haya, L.Y. Rusin, U. Tappe, J.P. Toennies, F.J. Aoiz, L. Banares, Chem. Phys. 207 (1996) 227.
[23] M. Faubel, B. Martínez-Haya, L.Y. Rusin, U. Tappe, J.P. Toennies, J. Phys. Chem. 101 (1997) 6415.
[24] M. Baer, M. Faubel, B. Martínez-Haya, L.Y. Rusin, U. Tappe, J.P. Toennies, K. Stark, H.-J. Werner, J. Chem. Phys. 104 (1996) 2743.
[25] M. Baer, M. Faubel, B. Martínez-Haya, L. Y Rusin, U. Tappe, J.P. Toennies, J. Chem. Phys. (1998) in press.
[26] F.J. Aoiz, L. Banares, V.J. Herrero, V. Saez Rabanos, K. Stark, H.-J. Werner, J. Phys. Chem. 98 (1994) 10665.
[27] F.J. Aoiz, L. Banares, M. Faubel, B. Martínez-Haya, L.Y. Rusin, U. Tappe, J.P. Toennies, Chem. Phys. 207 (1996) 245.
[28] B. Martínez-Haya, Thesis, Göttingen, 1996.
[29] J.M. Launay, M. Le Dourneuf, Chem. Phys. Lett. 163 (1989) 178.
[30] B. Lepetit, J.M. Launay, J. Chem. Phys. 95 (1991) 5159.
[31] J.M. Launay, M. Le Dourneuf, Chem. Phys. Lett. 163 (1989) 178.
[32] D.E. Manolopoulos, J. Chem. Phys. 85 (1986) 6425.
[33] J.M. Launay, S.B. Padkjær, Chem. Phys. Lett. 181 (1991) 95.